Differential Regulation of Action Potentials by Inactivating and Noninactivating BK Channels in Rat Adrenal Chromaffin Cells

Liang Sun,[†] Yu Xiong,[†] Xuhui Zeng,[‡] Ying Wu,[†] Na Pan,[†] Christopher J. Lingle,[‡] Anlian Qu,[†*] and Jiuping Ding[†*]
[†]Key Laboratory of Molecular Biophysics of the Ministry of Education, Huazhong University of Science and Technology, Wuhan, Hubei, China; and [‡]Department of Anesthesiology, Washington University School of Medicine, St. Louis, Missouri

ABSTRACT Large-conductance Ca^{2+}-activated K^+ (BK) channels can regulate cellular excitability in complex ways because they are able to respond independently to two distinct cellular signals, cytosolic Ca^{2+} and membrane potential. In rat chromaffin cells (RCC), inactivating BK_i and noninactivating (BK_s) channels differentially contribute to RCC action potential (AP) firing behavior. However, the basis for these differential effects has not been fully established. Here, we have simulated RCC action potential behavior, using Markovian models of BK_i and BK_s current and other RCC currents. The analysis shows that BK current influences both fast hyperpolarization and afterhyperpolarization of single APs and that, consistent with experimental observations, BK_i current facilitates repetitive firing of APs, whereas BK_s current does not. However, the key functional difference between BK_i and BK_s current that accounts for the differential firing is not inactivation but the more negatively shifted activation range for BK_i current at a given $[Ca^{2+}]$.

INTRODUCTION

Ca^{2+}- and voltage-dependent K^+ (BK) channels are widely expressed ion channels, but our understanding of the precise role that BK channels play in regulating cellular excitability remains incomplete. The specific role that BK channels play in sculpting cellular electrical activity often depends not only on the specific properties of the BK channels, but also on aspects of Ca^{2+} regulation and other ion channels. Among different cells, BK channels exhibit substantial functional differences, arising from factors that include alternative splice variants of the α subunit (1–3), tissue-specific expression of auxiliary β subunits (4), splice-variant-specific covalent modifications (5), and perhaps cell-specific association with other proteins (6). As a consequence, BK channels can differ in apparent Ca^{2+} dependence and kinetic properties, such that cells may differ with regard to the rates of BK-channel-mediated repolarization, rapidity of BK channel activation, and durations and magnitude of Ca^{2+}-mediated afterhyperpolarizations. It has been shown that among different cell types, BK channels promote the occurrence of plateau potentials (7), participate in action potential broadening (8), promote repetitive firing (9,10), and contribute to action potential repolarization and brief afterhyperpolarizations (8,9). Yet how specific biophysical properties of BK channels in a given cell may account for specific effects on excitability remains a topic of investigation. For example, dependent on the Ca^{2+} sensitivity of BK channels in a given cell, the range of voltages and submembrane Ca^{2+} found in the cell, and other voltage-dependent K^+ conductances, the physiological consequences of BK activation might differ in substantive ways. Thus, the functional role of BK channels in any given cell will depend not only on BK channel properties but also on the interplay of BK currents with other conductances that together shape the time course and extent of voltage trajectories and Ca^{2+} elevations.

Rat adrenal medullary chromaffin cells (RCCs) provide an interesting system in which to examine the potential physiological roles of different BK channel variants. The repetitive firing of action potentials (APs) in RCCs leads to the elevation of intracellular Ca^{2+}, which triggers secretion of catecholamines (11,12). Furthermore, the specific firing patterns of APs may influence secretory responses (13) and may be physiologically regulated (10,14). Previous work has shown that, dependent on the presence of two specific BK channel variants, an inactivating variant (termed BK_i) and a noninactivating variant (termed BK_s), RCCs exhibit differential firing behaviors in response to current injection (9,15). For RCCs, an essentially full set of ionic conductances has been identified that includes a TASK-mediated leak K^+ conductance (16), voltage-dependent Na^+ current (17), voltage-dependent Ca^{2+} current (18), voltage-dependent K^+ current (19–21), small-conductance Ca^{2+}-dependent SK-type K^+ current (22,23), and the two distinct types of BK current (9,24). Although complete kinetic descriptions of all currents are not available, each current has been sufficiently well described that simplified kinetic models can be defined that provide reasonable recapitulations of the native currents. Thus, RCCs provide a system in which the specific contributions of different currents to electrical behavior can be examined in a computational fashion.

Here, we provide empirical descriptions of the known components of RCC membrane currents and utilize them in simulations of the voltage behavior of an idealized RCC under current-clamp. We compare two cell models, one with BK_i current and one with BK_s current. The simulated

Submitted December 30, 2008, and accepted for publication June 30, 2009.

Liang Sun, Yu Xiong, and Xuhui Zeng contributed equally to this work.

*Correspondence: jpding@mail.hust.edu.cn or alqu@mail.hust.edu.cn

Editor: Richard W. Aldrich.

0006-3495/09/10/1832/11 $2.00

doi: 10.1016/j.bpj.2009.06.042

voltage behaviors demonstrate that, consistent with the behavior of native RCCs, model cells with BK_i currents are better able to fire repetitively during depolarizing constant-current injection, whereas model cells with BK_s currents fire in a phasic fashion. Furthermore, this analysis establishes that BK_i current supports repetitive firing not because of inactivation, but because of a more negatively shifted range of activation of BK_i channels compared to BK_s channels.

MATERIALS AND METHODS

Chromaffin cell preparation

Rat chromaffin cells were isolated as described previously (22). Briefly, chromaffin cells were dispersed from adrenal medullas isolated from two to three rats aged ~2–3 months. Isolated cells were cultured with Dulbecco's modified Eagle's medium (DMEM) in a standard CO_2 incubator at 37°C and 5% CO_2 and used for experiments in 2–6 days.

Expression in *Xenopus* oocytes

Xenopus laevis oocytes (stage IV) were harvested for injection as described in previous work (25). The mSlo1 α and $\beta 2$ auxiliary subunits were identical to those described in previous work (25,26). A total of 0.1–0.5 ng cRNA was injected into stage IV *Xenopus* oocytes with a ratio of $\alpha/\beta 2 = 1{:}2$ by weight, ensuring a large molar excess of β subunit RNA. Oocytes were used 3–5 days after injection of cRNA.

Electrophysiology

Whole-cell recordings from RCCs utilized the perforated-patch method (27). Series resistance was in the range 8–15 MΩ, of which 80–90% was electronically compensated. For BK channel recordings in oocytes, inside-out patches were bathed with constantly flowing solutions of defined Ca^{2+} from a multibarrel local application system. All currents were typically digitalized at 20 kHz and filtered at 5 kHz (Bessel low-pass filter; −3 dB) during digitization. For action potential experiments, all recordings were performed using the current-clamp capabilities of the Axopatch amplifier. All experiments were performed at room temperature (22–25°C).

Solutions

Electrophysiological recordings of BK channels were performed after 2–7 days incubation of oocytes in ND-96 (containing (in mM) 96 NaCl, 2.0 KCl, 1.8 $CaCl_2$, 1.0 $MgCl_2$, and 5.0 HEPES, pH 7.5) supplemented with sodium pyruvate (2.5 mM), penicillin (100 U/ml), streptomycin (100 mg/ml), and gentamicin (50 mg/ml). For inside-out patch recordings, the pipette extracellular solution contained (in mM) 140 potassium methanesulphonate, 20 KOH, 10 HEPES, and 2 $MgCl_2$, pH 7.0. The cytosolic solution contained (in mM) 140 potassium methanesulphonate, 20 KOH, and 10 HEPES, pH 7.0, and one of the following (in mM): 5 EGTA (for nominally 0 Ca^{2+}, and 0.5-, 1-, and 4-μM Ca^{2+} solutions), 5 HEDTA (for 10 μM Ca^{2+} solution), 10 HEDTA (for 60 μM Ca^{2+} solution) or no added Ca^{2+} buffer (for 100 μM and higher Ca^{2+}), as defined by the EGTAETC program (E. McCleskey, Vollum Institute, Portland, OR).

The normal bath saline for perforated patch-clamp experiments contained (in mM) 150 NaCl, 5.4 KCl, 10 HEPES, 1.8 $CaCl_2$, and 2.0 $MgCl_2$, pH 7.4, adjusted with *N*-methylglucamine. For the 0 Ca^{2+} normal saline, 2 mM Mg^{2+} was substituted for 1.8 mM Ca^{2+} into normal saline. For perforated patch-clamp recordings, the pipette solution contained (in mM), as described previously (28), 120 K-aspartate, 30 KCl, 10 HEPES (H^+), and 2 $MgCl_2$ titrated to pH 7.4 with *N*-methylglucamine, with amphotericin and pluronic acid included for permeabilization (27). For all RCC recordings, 200 nM apamin was added to extracellular solutions to block small-conductance Ca^{2+}-activated K^+ (SK) currents. In a similar way, 200 nM tetrodotoxin was used to reduce voltage-dependent Na^+ current. All salts and chemicals were obtained from Sigma-Aldrich (St. Louis, MO).

Data analysis

Data were analyzed with IGOR (Wavemetrics, Lake Oswego, OR), Clampfit (Molecular Devices, Sunnyvale, CA), SigmaPlot (SPSS Science, Chicago, IL). The fractional value of activation or steady-state inactivation was generated from the peak value of inactivating current or the steady-state value for noninactivating current and fit with a single Boltzmann function of the form

$$f(V) = (1 + \exp((V - V_{50})/k))^{-1}, \quad (1)$$

where V_{50} is the voltage at which the $f(V) = 0.5$, and κ is a factor reflecting the steepness of the activation curve or the steady-state inactivation curve. Fractional recovery curves of inactivating currents were fitted to an exponential function as follows:

$$I/I_{max} = 1 - \exp(-t/\tau_r). \quad (2)$$

Here τ_r is the recovery time constant. Unless stated otherwise, all data are presented as the mean ± SD.

Mathematical modeling and simulations

The differential equations for the kinetic modeling were solved numerically, using a fifth-order Runge-Kutta integration method. The integrating routines were written and executed with software CeL (Huazhong University of Science and Technology, Wuhan, Hubei, China), compiled with the C++ compiler to run under Windows XP.

RESULTS

We begin with empirical definitions of the kinetic properties of several of the main current components of rat chromaffin cells, specifically including I_{Na}, I_{Ca}, I_{Kv}, BK_i, and BK_s currents. We omit Ca^{2+}-dependent SK current, since experiments comparing the impact of BK current on RCC firing behavior were done in the presence of apamin (9). We begin with definitions of a model and a set of gating parameters for each current component, with the aim of providing a reasonable approximation of the native current in RCCs. We then simulate current clamp behavior during brief or more sustained current injection to determine whether the properties of the two kinds of BK current account for differences in firing behavior.

Definition of Na current

Voltage-dependent Na^+ current is the predominant inward current in RCCs (11), likely arising from $Na_V1.7$ and $\beta 1/\beta 3$ subunits (29). For RCC Na^+ current, we utilized a model containing 12 states (30), the parameters of which are given in Fig. S1 of the Supporting Material. Parameters were determined based on properties of channels arising from $Na_V1.7$ and $\beta 1/\beta 3$ subunits (see Table S1). Activation and inactivation behaviors of the simulated Na^+ current are summarized in Fig. S1 *B*. The normalized fractional activation curve

gives a half-maximal activation voltage (V_{50}) of −17.5 mV with slope κ = 5.2 mV; for fractional availability, V_{50} is −39.8 mV with slope κ = 3.4 mV (Fig. S1 *C*). The simulated Na^+ current inactivation time constant (τ_i) is 1.5 ms at −10 mV (Fig. S1 *C*). The recovery time constants at various membrane potentials (Fig. S1 *D*) are also consistent with previous results for Na^+ currents in RCCs (11).

Definition of voltage-gated K current

The molecular identities of voltage-dependent K^+ in RCCs remain incompletely defined, although multiple types of Kv channels have been described in bovine chromaffin cells (19). Some evidence suggests the involvement of two distinct subunits, Kv1.2 and Kv1.5, which may participate in mediating oxygen sensitivity of RCC K^+ currents as either homomultimers or heteromultimers (20,21,31,32). Both subunits result in channels of generally similar properties (33,34), although the activation properties of each can be subject to regulation (33,35). Here, we assume a single component of Kv current with properties similar to those of Kv1.2, with a half-maximal activation voltage of V_{50} = −4.3 mV and an activation time constant (τ_a) of 6 ms at 20 mV (34,36). For the simulation of Kv current, we utilized a linear five-state activation model with parameters given in Fig. S2 *A*. The simulated currents yielded V_{50} = −0.8 mV for activation, which is close to the V_{50} of Kv1.2 current (Fig. S2).

Definition of Ca^{2+} current and cytosolic Ca^{2+}

A variety of high-voltage-activated (HVA) calcium channels have been identified in adult RCCs (18,37). We ignore a low-voltage-activated (LVA) calcium current identified in embryonic chromaffin cells (38). To avoid iterative calculation of each HVA component, we utilize a single HVA Ca^{2+} current (39) whose gating model and parameters (Table S2) are defined in Fig. S3 *A*. Based on earlier work (18), the V_h for HVA calcium current in RCC was −3 mV (κ = 9 mV), with an activation time constant (τ_a) of ~1 ms at +10 mV (18). Simulated currents (see examples in Fig. S3) yielded a V_{50} = 2.3 mV (κ = 6 mV).

In modeling cellular electrical properties, it is important to include a procedure for relating Ca^{2+} influx to cellular Ca^{2+} concentrations. BK_i channels colocalize to some extent with HVA channels both in RCCs and elsewhere (6,18,37,40–43). Yet all BK channels in a cell may not be identically coupled to Ca^{2+} channels, and distinct BK channel variants may be coupled to different sets of HVA Ca^{2+} channels. For RCCs, the available evidence suggests that most BK channels are sufficiently close to Ca^{2+} channels to sense local Ca^{2+} increases during brief depolarizations (37). For the purposes of this study, we have assumed that activation of all BK channels by Ca^{2+} depends strictly on net influx and local diffusion of Ca^{2+} near individual Ca^{2+} channels. As such, we have employed a formulation first utilized by Beeler and Reuter (44) to convert Ca^{2+} influx to a local Ca^{2+} concentration:

$$\frac{d[\mathrm{Ca}]_i}{dt} = e_{\mathrm{trans}} \times I_{\mathrm{Ca}} - e_{\mathrm{diff}} \times [\mathrm{Ca}]_i, \qquad (3)$$

where e_{trans} is an arbitrary transfer coefficient that scales calcium influx to the calcium concentration, and e_{diff} is the calcium diffusion coefficient.

Kinetic properties of BK_s channels

Completely inactivating BK_i channels and the noninactivating BK_s channels largely segregate among different RCCs, although some cells of mixed phenotype can be found (9,24). The BK_s current is thought to arise from channels containing only four Slo1 α subunits. BK_i channels arise from the coassembly of four Slo1 α subunits and up to four auxiliary β2 subunits (26,45). We characterize BK_i cells as those that express almost exclusively BK_i current, whereas BK_s cells are those that express almost exclusively BK_s current.

The kinetic and steady-state properties of nonactivating BK current have been well studied in several laboratories (46,47). Rather than employ a full BK gating scheme (46,47), we have utilized the 10-state Monod-Wyman-Changeux kinetic model (47) shown in Fig. S4 *A*. This model includes four Ca^{2+}-binding steps, with all the voltage dependence assigned to the transitions between closed and open states, i.e., the C-O equilibrium. Simulations with this model result in predicted currents (Fig. S4) that closely reproduce the features of BK_s current in RCCs.

Kinetic properties of BK_i channels

Although a BK_i channel can have up to four β2 subunits, the average number of β2 subunits/channel in RCCs is ~3 (24). Here, we assume that each BK_i channel has four β2 subunits. This results in only a small difference in inactivation rate and level of steady-state inactivation compared to a population of native BK_i channels, each containing an average of three β2 subunits (24,45). Although many properties of $\alpha + \beta$2 currents have been defined previously (26,48), to obtain a more complete description of $\alpha + \beta$2 currents, we recorded from excised patches from oocytes to define activation (Fig. S5 *A1*), steady-state inactivation (Fig. S5 *A2*), and deactivation (Fig. S5 *A3*) of these currents. The overall dependence of BK_i current activation on Ca^{2+} and the shift in steady-state inactivation as a function of Ca^{2+} was defined over the range 0–60 μM Ca^{2+} (Fig. S5, *B1* and *B2*) (18). The instantaneous current-voltage properties determined (Fig. S5 *B3*) showed that net current at +100 mV is around two times that at −100 mV (49). Inactivation (Fig. S5 *C1*), activation, and deactivation (Fig. S5 *C2*) time constants were also defined, and the properties of recovery from inactivation at different voltages were determined (Fig. S5 *D*).

Inactivation of BK channels mediated by β2 subunits involves a two-step process in which a preinactivated open

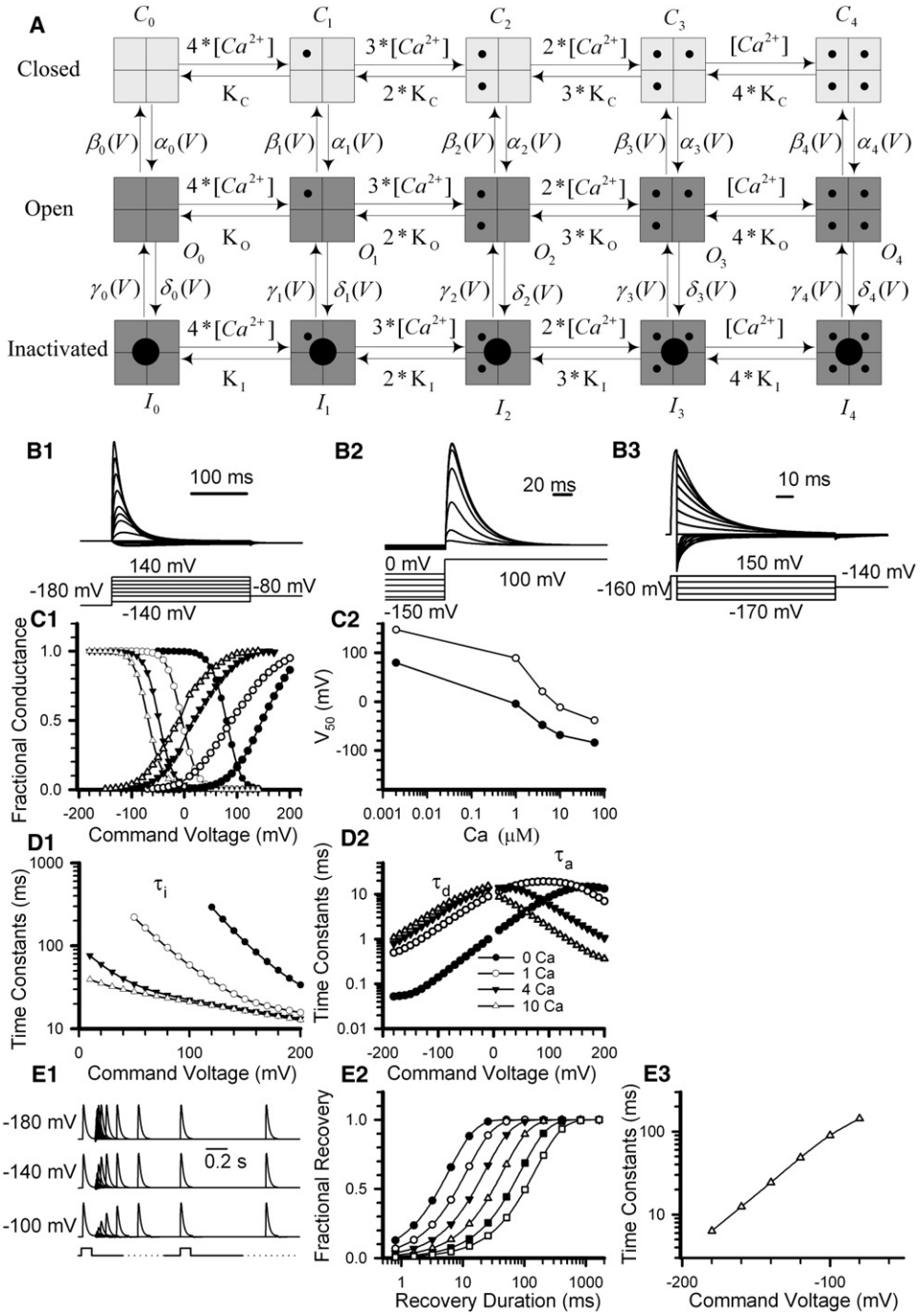

FIGURE 1 Properties of simulated BK_i currents. (*A*) The scheme summarizes a 10-state activation model for BK_i gating composed of four Ca^{2+} binding steps with voltage dependence assigned to the closed-to-open conformational step. The scheme includes a single-step inactivation process from the open states. Transition rates are defined in Table 1. (*B*) Standard voltage protocols were used to generate simulated current traces, allowing definition of activation behavior (*B1*), steady-state inactivation properties (*B2*), and deactivation behavior (*B3*) of BK_i currents. Simulation conditions assumed symmetrical 160 mM K^+ solution, and 10 μM internal Ca^{2+}. Currents in *B* were scaled by the instantaneous I/V generated from native $\alpha + \beta 2$ currents (Fig. S5). (*C1*) Fractional conductance and fractional availability are plotted as a function of membrane potential, based on measurements of BK_i currents. Solid lines are fits to the Boltzmann equation (Eq. 1). Curves correspond to Ca^{2+} concentrations of ~2 nM (*solid circles*), 1 μM (*open circles*), 4 μM (*inverted triangles*) and 10 μM (*triangles*). (*C2*) The V_{50} of activation (*open circles*) and steady-state inactivation (*solid circles*) are plotted as a function of $[Ca^{2+}]$ based on the simulated BK_i currents. The V_{50} values for activation and steady-state inactivation are 147.4 and 79.9 mV in 2 nM Ca^{2+}, 89.4 and −4.5 mV in 1 μM Ca^{2+}, 20.7 and −48.0 mV in 4 μM Ca^{2+}, −11.9 and −68.3 mV in 10 μM Ca^{2+}, and −38.2 and −84.0 mV in 60 μM Ca^{2+}. (*D1*) Inactivation time constants (τ_i) of simulated BK_i current are plotted as a function of voltage for 2 nM (*solid circles*), 1 μM (*open circles*), 4 μM (*inverted triangles*), and 10 μM (*triangles*). (*D2*) Deactivation time constants (τ_d) and activation time constants (τ_a) are plotted as a function of potential for 2 nM (*solid circles*), 1 μM (*open circles*), 4 μM (*inverted triangles*), and 10 μM (*triangles*). (*E1*) Traces show the time course of recovery from inactivation of simulated BK_i channels elicited by a paired-pulse protocol (activation steps to 100 mV) separated by steps of different duration to −180, −140, and −100 mV. (*E2*) The fractional recovery of BK_i channels is plotted as a function of recovery duration for −180, −160, −140, −120, −100, and −80 mV in 10 μM Ca^{2+}. Solid lines were fitted to Eq. 2. Recovery time constants (τ_r) are 6.4, 12.4, 24.4, 48.4, 89.4, and 143.9 ms at −180, −160, −140, −120, −100, and −80 mV, respectively. (*E3*) Recovery time constants are plotted as a function of recovery voltage at 10 μM internal Ca^{2+}.

state precedes the fully inactivated state, C-O-O*-I, where C, O, O*, and I are the closed, open, preinactivated-open, and inactivated states, respectively (50). Here, for simplicity, we use a one-step inactivation model (C-O-I; Fig. 1 *A*). An unusual aspect of BK_i current inactivation is that inactivated channels can recover from inactivation without reopening (51,52). This aspect of BK_i behavior is not incorporated in the model described here and might impact on the net BK_i current flux during tail currents. Table 1 lists the parameters used for simulation of BK_i currents. Constants for BK_i activation and deactivation differ from those used for BK_s simulations, because at any given $[Ca^{2+}]$ above ~1 μM, activation of channels containing $\beta 2$ subunits is shifted to more negative voltages than for those not containing $\beta 2$ subunits (26,53).

TABLE 1 Parameters used for current simulations in BK_i cells

$\alpha_n = A_n * \exp(z_{CO}FV/RT)\ s^{-1}$		$\beta_n = B_n * \exp(-z_{OC}FV/RT)\ s^{-1}$	
A_0	1	B_0	810
A_1	2	B_1	135
A_2	12	B_2	67.5
A_3	120	B_3	56.25
A_4	288	B_4	11.25
z_{CO}	0.513	z_{OC}	0.5745
$\delta_n = C_n * \exp(z_{OI}FV/RT)\ s^{-1}$		$\gamma_n = D_n * \exp(-z_{IO}FV/RT)\ s^{-1}$	
C_0	15	D_0	7.000
C_1	18	D_1	3.360
C_2	21	D_2	1.568
C_3	25	D_3	0.7468
C_4	30	D_4	0.3584
z_{OI}	0.1293	z_{IO}	0.8617
K_C	7.2	K_O	0.6
K_I	0.24		
Ca^{2+} on-rates per site		$10^9\ M^{-1}\ s^{-1}$	
Ca^{2+} off-rates from C_n per binding site		$10^9 K_C$ (6,600 s^{-1})	
Ca^{2+} off-rates from O_n per binding site		$10^9 K_O$ (550 s^{-1})	
Ca^{2+} off-rates from I_n per binding site		$10^9 K_I$ (220 s^{-1})	

TABLE 2 Model cell parameters

Channel	G_{max} (nS)	Reversal potential (mV)
Na	54	55
Kv	1.5	−70
BK_S/BK_i	90	−60
Ca	1	60
Leak	0.45	−55
Ca^{2+} transition coefficient		0.006 $\mu M\ pA^{-1}\ ms^{-1}$
Ca^{2+} diffusion coefficient		0.004 ms^{-1}
Global intracellular $[Ca^{2+}]_i$		10 nM
V_{Rest}		−55 mV

Model cell was 15 μm in diameter, with a membrane capacity of $C_m = 10$ pF.

Simulated BK_i currents (Fig. 1 *B*) were generated with voltage protocols identical to those used to define gating properties of expressed $\alpha + \beta 2$ currents (Fig. S5). In these simulated BK_i currents, the voltage dependence of conductance, the shift in steady-state inactivation with voltage, and the general behavior of the V_{50} both for activation and steady-state inactivation (Fig. 1 *C*) closely mirrored those of the native BK_i currents (Fig. S5 *B*). Furthermore, τ_a and τ_d for the simulated BK_i currents (Fig. 1 *D*) provided reasonable approximations of the behavior of experimentally measured BK_i currents (Fig. S5 *C*). The simulated BK_i currents also exhibited a voltage dependence of recovery from inactivation (Fig. 1 *E*) similar to that observed in the native BK_i currents (Fig. S5 *D*). Thus, these gating behaviors of both the simulated BK_i and BK_s currents seem sufficiently close to native currents to allow their impact on current clamp behavior to be assessed.

Characterization of the AP firing behavior in an RCC first requires identification of the principle BK current component in that cell (9). To accomplish this, a direct step to +90 mV in an RCC typically activates very little, if any, BK current, since net Ca^{2+} influx at that potential is negligible. Therefore, comparison of currents at +90 mV, either with or without a conditioning step, to a potential that results in robust Ca^{2+} elevation was used in native RCCs to provide clear visualization of whether the BK current exhibits inactivation (BK_i) or very slow decay (BK_s), reflecting Ca^{2+} clearance (9).

Patterns of AP firing in response to constant-current injection in native and model RCCs

The two distinct patterns of repetitive AP firing during 2-s current injections in BK_s and BK_i cells (9) suggest that BK current properties determine the differences between the two cell types. We therefore utilized model cells, with parameters defined in Table 2, to test whether the type of BK current might account for the current clamp behavior. For both BK_i and BK_s model cell simulations, all parameters except BK channel gating properties were identical. Model cell simulations of AP behavior were calculated from Eqs. A1 and A2 (see the Appendix in the Supporting Material) and Eq. 3. Values of conductance for each channel type were selected to yield conductances in the current-clamp simulations that compared with those evoked by AP clamp voltage commands in experiments on native cells. The instantaneous rectification of BK_i current was ignored in these simulations, since the instantaneous I/V relationship is largely linear from −60 to +60 mV.

In response to different levels of current injection (Fig. 2 *A*), the BK_i model cell exhibited a somewhat accommodating repetitive firing, whereas the BK_s model cell exhibited a phasic response with only one or a few APs. The number of APs over 0 mV increased with the amount of injected current in the BK_i model cell, whereas the number in the BK_s model cell initially increased and then decreased (Fig. 2 *B*). This behavior approximates that observed in native RCCs (9). In the model cell with BK_i current, the afterhyperpolarizations between APs are better able to return the potential to near-resting potentials, which presumably has a major impact on the availability of voltage-dependent Na^+ current for subsequent APs. This probably results from the fact that BK_i current is more effectively activated at a given $[Ca^{2+}]$ and voltage, resulting in more prolonged tail current at a given voltage and $[Ca^{2+}]$. The persistence of the membrane potential of the BK_s model cell at more depolarized levels during current injection is also consistent with previously reported results (9).

We compared the impact of these current-clamp behaviors on cytosolic Ca^{2+} using Eq. 3. It should be kept in mind that Eq. 3 does not provide a physically realistic estimate of $[Ca^{2+}]_i$, but rather gives a relative value that allows Ca^{2+} influx to be scaled to BK current activation, based on the assumption that all BK channels are sampling this same concentration of Ca^{2+}. However, as long as BK_i and BK_s channels are organized similarly with regard to Ca^{2+} channels, Eq. 3 provides a meaningful comparison of relative

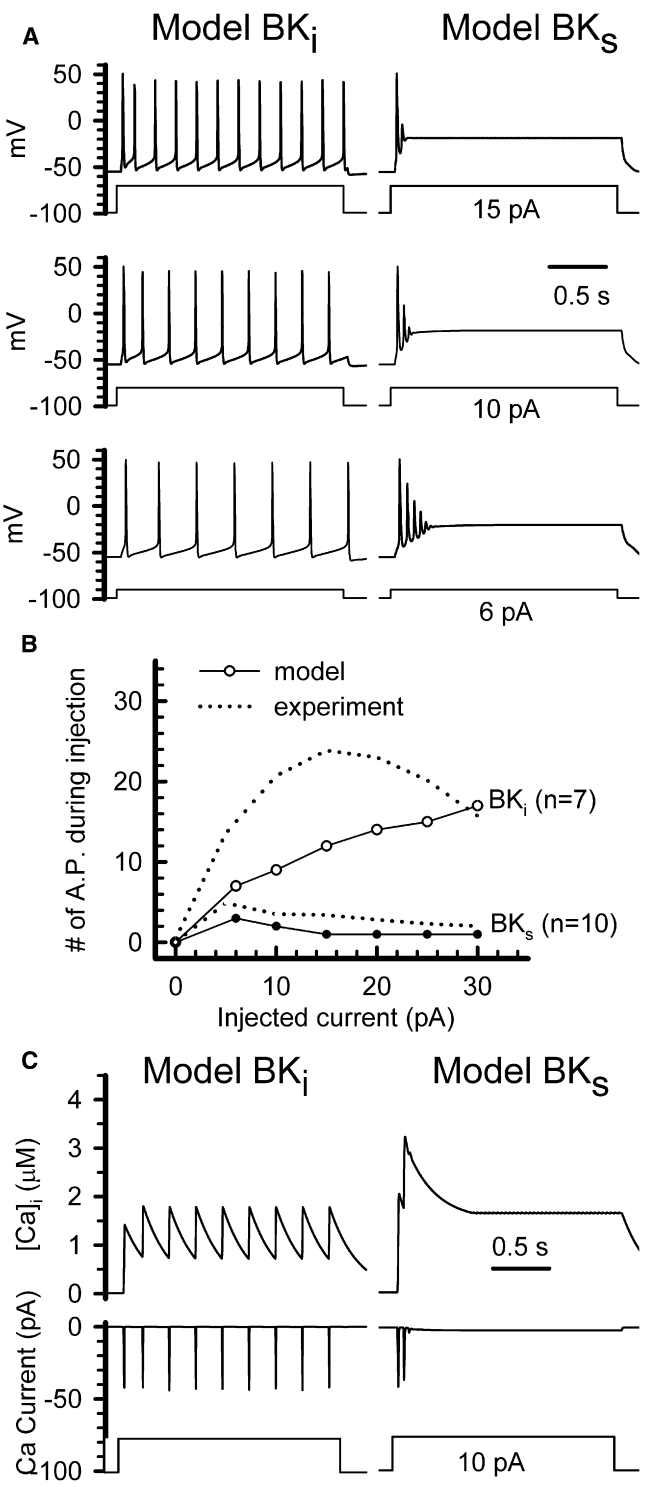

FIGURE 2 BK$_i$ and BK$_s$ currents differentially contribute to AP firing in model cells. (*A*) Model cells containing either BK$_i$ (*left*) or BK$_s$ (*right*) current were used to simulate action potentials in response to constant-current injection of different amplitude (*lower*, 6 pA; *middle*, 10 pA; *upper*, 20 pA). The resting potential was −55 mV. (*B*) The number of action potentials elicited during a 2-s period of injected current are plotted as a function of the amplitude of injected current for model BK$_i$ (*open circles*) or model BK$_s$ (*solid circles*) cells. The dotted lines correspond to experimental results obtained previously (9) in native RCCs. (*C*) *Left*: The upper trace shows the simulated time course of the local calcium concentration in a model BK$_i$ cell; the middle traces shows calcium currents activated by an injected current of 10 pA in the model BK$_i$ cell (*lower trace*). *Right*: The upper trace shows the time course of the local calcium concentration in a BK$_s$ model cell, whereas the middle trace shows calcium currents activated in the BK$_s$ model cell by an injected current of 10 pA (*lower trace*).

increases in Ca^{2+} in the two types of model cells (Fig. 2 *C*). In both model cells, the Ca^{2+} concentration rapidly increases to 1–3 μM after a few APs, which is consistent with observations by others (54). In the BK$_i$ model cell, the simulation reveals a distinct rise and fall between individual APs, with little diminution in peak Ca^{2+} current influx. In contrast, in the BK$_s$ model cell, Ca^{2+} is maintained at a higher level due to a small sustained calcium influx through HVA Ca^{2+} channels that appears at ~−25 mV. This sustained Ca^{2+} level is maintained despite the reduction of peak Ca^{2+} current per action potential that occurs as peak action potential is diminished.

The Ca^{2+} dependence of AP firing in native RCCs and simulated model cells

The Ca^{2+} dependence of repetitive AP firing in native BK$_i$ or BK$_s$ RCCs was examined through application of 0-Ca^{2+} saline (Fig. 3 *A*) in the presence of 200 nM apamin to block SK currents. In both cell types, removal of external Ca^{2+} reduced the response to injected current to one or two APs, indicating that the ability to fire repetitive APs in both BK$_i$ and BK$_s$ cells is Ca^{2+}-dependent. In model BK$_i$ and BK$_s$ cells, when both SK and BK current are excluded from the simulations, the number of APs evoked by 10 pA constant-current injection was similarly reduced to one or two APs (Fig. 3 *B*). The ability to fire repetitively will also potentially be influenced by Kv current density (see Fig. 5). In our model cells, Kv current density is small relative to the maximal BK current (see Table 2) because of the small amplitude of Kv current relative to BK current observed in voltage-clamp experiments in both BK$_i$ and BK$_s$ cells (9). The inability of either native BK$_i$ or BK$_s$ cells to fire repetitively in 0 Ca^{2+} is also indicative that the Kv current density is low.

Contributions of BK current to AHPs in native and model BK$_i$ and BK$_s$ cells

We next examined the Ca^{2+} dependence of afterhyperpolarizations (AHPs) after single APs in either native or model cells. In native RCCs, single APs were elicited by a brief 100-pA depolarizing current pulse and examined with either 1.8 or 0 mM extracellular Ca^{2+} saline (with 200 nM apamin to block SK current). In BK$_i$ cells, removal of external Ca^{2+} resulted in a pronounced slowing of repolarization, particularly in the second half of the repolarization. Furthermore, a small AHP after the AP was abolished in 0 Ca^{2+} (Fig. 4 *A*, *left*). In contrast, in BK$_s$ cells, there was little clear change in the AP waveform (Fig. 4 *A*, *right*), suggesting that there is little BK$_s$ current activation with a single AP.

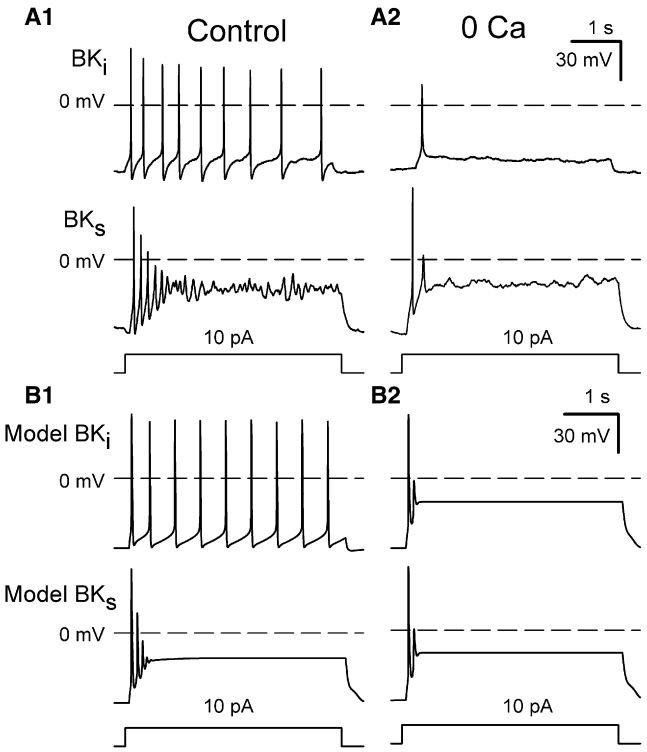

FIGURE 3 Repetitive AP firing in RCCs is abolished by 0 Ca^{2+}. (*A1*) Action potentials were elicited by constant-current injection in identified BK_i (*upper*) and BK_s (*lower*) RCCs using perforated-patch recording with normal extracellular (1.8 mM Ca^{2+}) saline. (*A2*) Traces were recorded in 0 Ca^{2+} normal saline (with 2 mM Mg^{2+}). In all cases, the extracellular saline contained 200 nM apamin. (*B1*) Action potentials activated by constant-current injection were simulated in BK_i (*upper*) and BK_s (*lower*) model cells. SK current was inactive. (*B2*) The traces were obtained from model simulations in which only Ca^{2+} current was removed from the simulation.

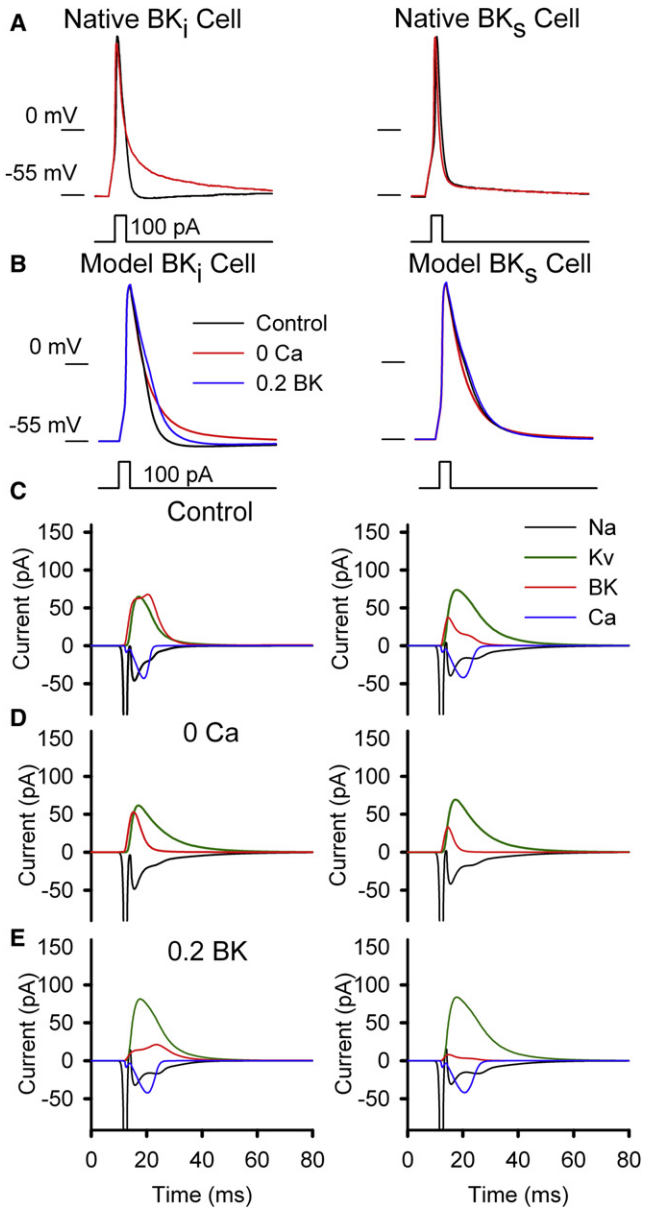

FIGURE 4 BK current differentially contributes to AP repolarization in BK_i and BK_s cells. (*A*) APs elicited by a 100-pA depolarizing current pulse are shown for identified BK_i (*left*) and BK_s (*right*) RCCs in both control and 0-Ca^{2+} saline, as indicated. The extracellular saline contained 200 nM apamin. (*B*) The simulated waveforms of APs elicited by 100-pA depolarizing current pulses are shown for a model BK_i (*left*) cell and a model BK_s (*right*) cell in control and 0 Ca^{2+}, as indicated. SK currents were removed in all cases. (*C–E*) Individual current components (Na, Kv, BK, and Ca) appearing in a single AP are shown for a model BK_i (*left*) cell and a model BKs (*right*) cell, for control saline (*C*), 0 Ca^{2+} saline (*D*), and with nominal 100 nM CTX (0.2 BK; *E*).

We also evoked single APs in BK_i and BK_s model cells (also with no SK current) and tested the consequences of Ca^{2+} removal. For the BK_i model cell, removal of Ca^{2+} current resulted in slowing of repolarization similar to that seen in the native RCCs, and the AHP after the AP was also abolished (Fig. 4 *B*, *left*). In contrast, for the BK_s model cell, with Ca^{2+} current removed, the AP repolarization actually became slightly faster (Fig. 4 *B*, *right*), presumably because of the removal of inward Ca^{2+} current during the later stages of the AP. The effect of ~100 nM charybdotoxin (CTX) (EC_{50} (half-maximal effective concentration) ~ 25 nM) (9) was also simulated by reducing the available BK current by 80%. For the BK_i model cell, the simulated AP exhibited a pronounced prolongation with only a minor effect in the BK_s model cell (Fig. 4 *B*). Both the 0-Ca^{2+} and simulated CTX effects closely mirror those seen in native RCCs (9). Specifically, CTX (0.2 BK) mediates a delay in repolarization immediately after the AP peak, whereas 0 Ca^{2+} only impacts on AP repolarization at late times in the decay process.

We next examined the contributions of each voltage-dependent current that is activated during the evoked APs in both the BK_i (Fig. 4 *C*, *left*) and BK_s (Fig. 4 *C*, *right*) model cells. The net BK current flux was substantially larger in the BK_i model cell, whereas the duration of Ca^{2+} current was clearly more prolonged in the BK_s model cell. In the BK_s model cell, the primary repolarizing current was mediated by Kv channel. When Ca^{2+} current was omitted

(Fig. 4 *D*), BK current in both cell types was diminished but still substantial. The relatively small reduction of BK current elicited by a single AP presumably reflects the ability of voltage alone to activate BK channels (46), particularly at early times during an AP. A contributing factor to the slow repolarization in BK_i cells with 0 Ca^{2+} appears to be the prominent secondary persistence of Na^+ current (Fig. 4 *D*, *left*). The BK_s model cell in normal saline also shows more persistence of Na^+ current (Fig. 4 *C*, *right*), consistent with the slower overall repolarization in the BK_s model cell. The ability of the simulated CTX effect to delay repolarization, in comparison to the effect of 0 Ca^{2+}, appears to arise because of the ability of CTX to block the early activation of BK current that occurs during the initial upswing of an AP.

Overall, the contribution of BK current to repolarization in BK_i and BK_s model cells closely mimics the contribution of these currents to native RCCs. The primary difference between native and model cells is that the model cells exhibit more prolonged AP durations, particularly in the BK_s model cell. The reasons for this difference will be examined in future iterations of this modeling effort, but contributing factors might include the density of BK channels, the density of Na^+ and Ca^{2+} channels, or the approximation made for coupling of Ca^{2+} influx to BK activation. It will be noted (Fig. 4, *C* and *D*) that Kv current contributes somewhat more prominently to net outward current in model BK_s cells than in BK_i cells, although both model cells contain the same number of BK channels. This presumably arises because the weaker BK activation in BK_s cells slightly delays repolarization, allowing for the enhanced activation of Kv current.

Inactivation is not responsible for the repetitive firing associated with BK_i channels

One proposed explanation for the difference in repetitive firing behavior between BK_i and BK_s cells is that the range of activation for BK_i current is more negatively shifted (15), allowing it to play a more prominent role in AHPs between APs. To test this idea, we compared the ability of BK_i current with inactivation intact to its ability with inactivated states removed. In response to depolarizing current injection, a simulation in which BK_i channels do not inactivate exhibits a slight increase in firing rate in comparison to the normal BK_i model cell (Fig. 5 *A*). This small increase in firing rate probably arises because of slightly stronger total BK activation in the absence of some very weak cumulative inactivation. We then added inactivated states to the model for BK_s current without changing any of the transitions between closed and open states. In response to constant-current injection, a model cell with inactivating BK_s channels exhibited a phasic firing behavior essentially identical to that of the standard BK_s model cell (Fig. 5 *B*). This directly confirms the idea that the key aspect of BK channels that supports repetitive firing in RCCs is not inactivation itself but the more negatively shifted range of activation produced by the $\beta 2$ subunit. Since

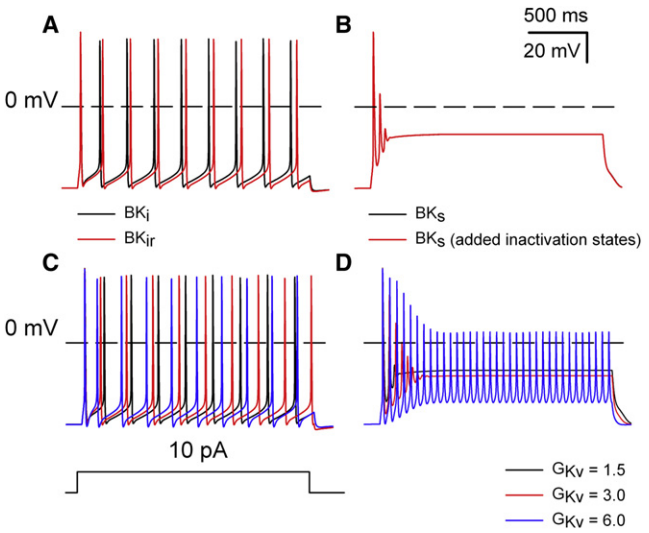

FIGURE 5 Ability of BK current in RCCs to support repetitive firing arises not from inactivation but from the shifted range of activation compared to BK_s current. (*A*) APs were elicited by a 2-s 10-pA current injection in the model BK_i cell either with inactivation intact (*black line*) or with transitions to inactivated states removed (*red line*). (*B*) APs were elicited by a 2-s 10-pA current injection either in the model BK_s cell (*black line*) or the model BK_s cell with inactivated states implemented (*red line*). (*C*) The density of Kv channels in the BK_i cell was increased from 1.5 to 3.0 and then 6.0, producing a slight increase in the AP firing rate. (*D*) An increase of Kv current density in a BK_s cell supports repetitive firing with reduced AP amplitude.

Kv channels are also expected to influence repetitive firing behavior, we also examined the ability of increases in Kv current density to influence repetitive firing in the BK_i and BK_s model cells (Fig. 5, *C* and *D*). Not unexpectedly, an increase in Kv current density, although it has little effect in the BK_i model cell, is able to support repetitive firing in the BK_s model cell. The absence of appreciable repetitive firing in native BK_s cells is therefore consistent with the modest amounts of Kv current densities used in our simulations.

DISCUSSION

We have examined whether the properties of inactivating and noninactivating BK channels predict the previously observed differential AP firing behavior among RCCs that contain either predominantly BK_i or BK_s current (9,15). The overall conclusion is that the presence of BK_i current contributes to the ability of a model BK_i cell to fire repetitively during constant current injection, whereas in model cells with exclusively BK_s current, constant current injection results in only one or very few APs. These differences arise, not because of the inactivation behavior of BK_i current, but from the more negatively shifted range of activation of BK_i channels at a given $[Ca^{2+}]_i$ in comparison to BK_s current. Specifically, the voltage activation curve for activation of BK channels arising from $\alpha + \beta 2$ subunits (26,53) is shifted to more negative values at a given Ca^{2+}. Because of this shift

in gating, BK_i channels better contribute to a robust afterhyperpolarization among APs, which presumably allows Na^+ channels to recover from inactivation and participate in repetitive firing. The ability of a shift in activation range of a K^+ channel to influence repetitive firing is not surprising, and others have observed that shifting the gating range of a Kv channel by even as little as 20 mV can impact substantially on the ability of a model cell to exhibit repetitive firing (10,55). The gratifying aspect of the simulations presented here is that model cells, based on plausible differences in BK channel properties, were able to reproduce the differential current-clamp properties of native BK_i and BK_s RCCs. Although it has been previously proposed that this might arise from the difference in activation properties of the two BK currents (9,15), the simulations presented here provide stronger support for this idea. A shift in BK gating properties, probably arising from a change in expression of Slo1 α-subunit splice variants, has also been shown to underlie changes in RCC firing properties after hypophysectomy (10).

The differences in range of activation of BK_i and BK_s current also contribute to other properties of native BK_i and BK_s cells. In both native and model cells with BK_i channels, after single evoked APs, BK channels contribute clearly to AP repolarization and afterhyperpolarizations, whereas in cells with BK_s current, very little BK current appears to be activated during single APs. This is consistent with differences in the effect of 0 Ca^{2+} or CTX application on afterhyperpolarizations in native BK_i and BK_s cells (9). Although both 0 Ca^{2+} and CTX have been observed to produce a slowing of repolarization in native BK_i cells, the effects are quite distinct (9). Whereas 0 Ca^{2+} results in a slowing of repolarization at later times in the AP decay time course, essentially abolishing the afterhyperpolarizations, CTX results in a delay in repolarization immediately after the peak of the AP. This behavior was nicely mimicked by the model BK_i cell. A powerful aspect of the simulation approach is that it provides a potential explanation for these differences by allowing examination of each individual current component during a simulation. This approach revealed that the differences between 0 Ca^{2+} and CTX arise because CTX more effectively blocks BK current during the initial upswing of the AP. Furthermore, in 0 Ca^{2+}, there is a secondary persistence of inward Na^+ current that contributes to the slow AP repolarization. We feel that neither the greater effect of CTX on early BK current nor the increased late Na^+ current in 0 Ca^{2+} would have seemed obvious factors contributing to the difference between effects of 0 Ca^{2+} and CTX. This highlights the potential power of realistic models of simulation guided by experiment.

Left unanswered by the analysis presented here is the physiological role of BK_i inactivation in RCCs. One potential role of inactivating BK channels has been proposed in regard to use-dependent spike prolongation both in hippocampal pyramidal cells (56) and also in neurons of the rat lateral amygdala (8). In both cases, AP broadening is fully developed within 3–5 action potentials and is favored by firing frequencies >20 Hz, indicative that any inactivating channel mediating these effects must exhibit a more rapid and complete inactivation than is typically observed for β2-mediated inactivation of BK channels in RCCs. The analysis presented here sheds no light on this question.

An important future improvement over the models used here will be the replacement of the 10-state gating model for BK_i and BK_s current activation with a more complete model of BK activation. Although this will be more computationally intensive, a complete allosteric model incorporating independent Ca^{2+} and voltage-dependent transitions (46) should allow a better approximation of the Ca^{2+}-dependence of activation and deactivation behavior for both BK_i and BK_s current. BK activation and deactivation time constants vary with [Ca^{2+}] in complex ways, particularly at Ca^{2+} <1 μM contingent upon activation of either of two distinct types of Ca^{2+} binding sites (57). This behavior cannot be readily approximated solely by the 10-state model. Furthermore, activation and deactivation are markedly slowed by the β2 subunit (4) in ways that should be better described by a more complete gating model. Although the models used here capture the essential differences in behavior between these two types of BK current, it will be interesting to know to what extent the observed effects on AP firing may arise not only from the equilibrium differences in V_h, but also specific differences in the Ca^{2+}-dependence of channel gating behavior.

A primary goal of this work was to build a simulation approach based on Markovian models of channel gating, rather the often used Hodgkin-Huxley formalisms. We have utilized a number of simplifying assumptions. First, detailed kinetic models and quantitative estimates of current densities for many of the underlying currents in RCCs are not yet available. When such information becomes available, more physically plausible models with appropriate kinetic rates can be easily implemented into the current approach. Second, we have treated different Ca^{2+} current components as a single entity driving elevations in local Ca^{2+}. Given the overlap in the ranges of voltage-dependence of activation and kinetic features of different HVA currents, this assumption seems acceptable. A circumstance in which specific definition of separate Ca^{2+} current components would be useful would be in cases where there is differential modulation of specific Ca^{2+} currents, perhaps with specific coupling to BK channels. Third, we have used a simple procedure for relating Ca^{2+} influx to effective $[Ca^{2+}]_i$ (44). Explicit calculation of [Ca^{2+}] in different submembrane compartments that takes into account cytosolic Ca^{2+} buffering and extrusion would allow a more realistic examination of how BK activation tracks cytosolic [Ca^{2+}]. However, in regards to the evaluation of the differential contribution of BK_i and BK_s current to AP firing, the assumptions used here seem acceptable. With further refinement of this model and the inclusion of additional data-based estimates of the properties of various current, this

approach promises to provide a useful evaluation of how different conductances impact on cellular excitability.

SUPPORTING MATERIAL

Five figures, three tables, an appendix, and references are available at http://www.biophysj.org/biophysj/supplemental/S0006-3495(09)01218-1.

This work was supported by grants from the National Science Foundation of China (30770522), the National Institutes of Health (GM081748 to C.L.), and the Program of Introducing Talents of Discipline to Universities (B08029).

REFERENCES

1. Saito, M., C. Nelson, L. Salkoff, and C. J. Lingle. 1997. A cysteine-rich domain defined by a novel exon in a slo variant in rat adrenal chromaffin cells and PC12 cells. *J. Biol. Chem.* 272:11710–11717.
2. Dworetzky, S. I., J. T. Trojnacki, and V. K. Gribkoff. 1994. Cloning and expression of a human large-conductance calcium-activated potassium channel. *Brain Res. Mol. Brain Res.* 27:189–193.
3. Tseng-Crank, J., J. A. Yao, M. F. Berman, and G. N. Tseng. 1993. Functional role of the NH2-terminal cytoplasmic domain of a mammalian A-type K channel. *J. Gen. Physiol.* 102:1057–1083.
4. Orio, P., P. Rojas, G. Ferreira, and R. Latorre. 2002. New disguises for an old channel: MaxiK channel β-subunits. *News Physiol. Sci.* 17:156–161.
5. Salkoff, L., A. Butler, G. Ferreira, C. Santi, and A. Wei. 2006. High-conductance potassium channels of the SLO family. *Nat. Rev. Neurosci.* 7:921–931.
6. Berkefeld, H., C. A. Sailer, W. Bildl, V. Rohde, J. O. Thumfart, et al. 2006. BKCa-Cav channel complexes mediate rapid and localized Ca^{2+}-activated K^+ signaling. *Science.* 314:615–620.
7. Van Goor, F., Y. X. Li, and S. S. Stojilkovic. 2001. Paradoxical role of large-conductance calcium-activated K^+ (BK) channels in controlling action potential-driven Ca^{2+} entry in anterior pituitary cells. *J. Neurosci.* 21:5902–5915.
8. Faber, E. S., and P. Sah. 2003. Ca^{2+}-activated K^+ (BK) channel inactivation contributes to spike broadening during repetitive firing in the rat lateral amygdala. *J. Physiol.* 552:483–497.
9. Solaro, C. R., M. Prakriya, J. P. Ding, and C. J. Lingle. 1995. Inactivating and noninactivating Ca^{2+}- and voltage-dependent K^+ current in rat adrenal chromaffin cells. *J. Neurosci.* 15:6110–6123.
10. Lovell, P. V., and D. P. McCobb. 2001. Pituitary control of BK potassium channel function and intrinsic firing properties of adrenal chromaffin cells. *J. Neurosci.* 21:3429–3442.
11. Lou, X. L., X. Yu, X. K. Chen, K. L. Duan, L. M. He, et al. 2003. Na^+ channel inactivation: a comparative study between pancreatic islet β-cells and adrenal chromaffin cells in rat. *J. Physiol.* 548:191–202.
12. Zhou, Z., and S. Misler. 1995. Action potential-induced quantal secretion of catecholamines from rat adrenal chromaffin cells. *J. Biol. Chem.* 270:3498–3505.
13. Duan, K., X. Yu, C. Zhang, and Z. Zhou. 2003. Control of secretion by temporal patterns of action potentials in adrenal chromaffin cells. *J. Neurosci.* 23:11235–11243.
14. Lovell, P. V., J. T. King, and D. P. McCobb. 2004. Acute modulation of adrenal chromaffin cell BK channel gating and cell excitability by glucocorticoids. *J. Neurophysiol.* 91:561–570.
15. Lingle, C. J., C. R. Solaro, M. Prakriya, and J. P. Ding. 1996. Calcium-activated potassium channels in adrenal chromaffin cells. *Ion Channels.* 4:261–301.
16. Inoue, M., K. Harada, H. Matsuoka, T. Sata, and A. Warashina. 2008. Inhibition of TASK1-like channels by muscarinic receptor stimulation in rat adrenal medullary cells. *J. Neurochem.* 106:1804–1814.
17. Fenwick, E. M., A. Marty, and E. Neher. 1982. Sodium and calcium channels in bovine chromaffin cells. *J. Physiol.* 331:599–635.
18. Prakriya, M., and C. J. Lingle. 1999. BK channel activation by brief depolarizations requires Ca^{2+} influx through L- and Q-type Ca^{2+} channels in rat chromaffin cells. *J. Neurophysiol.* 81:2267–2278.
19. Marty, A., and E. Neher. 1985. Potassium channels in cultured bovine adrenal chromaffin cells. *J. Physiol.* 367:117–141.
20. Conforti, L., and D. E. Millhorn. 1997. Selective inhibition of a slow-inactivating voltage-dependent K^+ channel in rat PC12 cells by hypoxia. *J. Physiol.* 502:293–305.
21. Conforti, L., I. Bodi, J. W. Nisbet, and D. E. Millhorn. 2000. O2-sensitive K^+ channels: role of the Kv1.2-subunit in mediating the hypoxic response. *J. Physiol.* 524:783–793.
22. Neely, A., and C. J. Lingle. 1992. Two components of calcium-activated potassium current in rat adrenal chromaffin cells. *J. Physiol.* 453:97–131.
23. Park, Y. B. 1994. Ion selectivity and gating of small conductance Ca^{2+}-activated K^+ channels in cultured rat adrenal chromaffin cells. *J. Physiol.* 481:555–570.
24. Ding, J. P., Z. W. Li, and C. J. Lingle. 1998. Inactivating BK channels in rat chromaffin cells may arise from heteromultimeric assembly of distinct inactivation-competent and noninactivating subunits. *Biophys. J.* 74:268–289.
25. Wei, A., C. Solaro, C. Lingle, and L. Salkoff. 1994. Calcium sensitivity of BK-type KCa channels determined by a separable domain. *Neuron.* 13:671–681.
26. Xia, X. M., J. P. Ding, and C. J. Lingle. 1999. Molecular basis for the inactivation of Ca^{2+}- and voltage-dependent BK channels in adrenal chromaffin cells and rat insulinoma tumor cells. *J. Neurosci.* 19:5255–5264.
27. Herrington, J., C. R. Solaro, A. Neely, and C. J. Lingle. 1995. The suppression of Ca^{2+}- and voltage-dependent outward K^+ current during mAChR activation in rat adrenal chromaffin cells. *J. Physiol.* 485:297–318.
28. Prakriya, M., C. R. Solaro, and C. J. Lingle. 1996. $[Ca^{2+}]_i$ elevations detected by BK channels during Ca^{2+} influx and muscarine-mediated release of Ca^{2+} from intracellular stores in rat chromaffin cells. *J. Neurosci.* 16:4344–4359.
29. Morgan, K., E. B. Stevens, B. Shah, P. J. Cox, A. K. Dixon, et al. 2000. β3: an additional auxiliary subunit of the voltage-sensitive sodium channel that modulates channel gating with distinct kinetics. *Proc. Natl. Acad. Sci. USA.* 97:2308–2313.
30. Kuo, C. C., and B. P. Bean. 1994. Na^+ channels must deactivate to recover from inactivation. *Neuron.* 12:819–829.
31. Thompson, R. J., and C. A. Nurse. 1998. Anoxia differentially modulates multiple K^+ currents and depolarizes neonatal rat adrenal chromaffin cells. *J. Physiol.* 512:421–434.
32. Fearon, I. M., R. J. Thompson, I. Samjoo, C. Vollmer, L. C. Doering, et al. 2002. O2-sensitive K^+ channels in immortalised rat chromaffin-cell-derived MAH cells. *J. Physiol.* 545:807–818.
33. Steidl, J. V., and A. J. Yool. 1999. Differential sensitivity of voltage-gated potassium channels Kv1.5 and Kv1.2 to acidic pH and molecular identification of pH sensor. *Mol. Pharmacol.* 55:812–820.
34. Grissmer, S., A. N. Nguyen, J. Aiyar, D. C. Hanson, R. J. Mather, et al. 1994. Pharmacological characterization of five cloned voltage-gated K^+ channels, types Kv1.1, 1.2, 1.3, 1.5, and 3.1, stably expressed in mammalian cell lines. *Mol. Pharmacol.* 45:1227–1234.
35. Rezazadeh, S., H. T. Kurata, T. W. Claydon, S. J. Kehl, and D. Fedida. 2007. An activation gating switch in Kv1.2 is localized to a threonine residue in the S2–S3 linker. *Biophys. J.* 93:4173–4186.
36. Neshatian, L., Y. M. Leung, Y. Kang, X. Gao, H. Xie, et al. 2007. Distinct modulation of Kv1.2 channel gating by wild type, but not open form, of syntaxin-1A. *Am. J. Physiol. Gastrointest. Liver Physiol.* 292:G1233–G1242.
37. Prakriya, M., and C. J. Lingle. 2000. Activation of BK channels in rat chromaffin cells requires summation of Ca^{2+} influx from multiple Ca^{2+} channels. *J. Neurophysiol.* 84:1123–1135.

38. Bournaud, R., J. Hidalgo, H. Yu, E. Jaimovich, and T. Shimahara. 2001. Low threshold T-type calcium current in rat embryonic chromaffin cells. *J. Physiol.* 537:35–44.

39. Li, L., J. Bischofberger, and P. Jonas. 2007. Differential gating and recruitment of P/Q-, N-, and R-type Ca^{2+} channels in hippocampal mossy fiber boutons. *J. Neurosci.* 27:13420–13429.

40. Loane, D. J., P. A. Lima, and N. V. Marrion. 2007. Co-assembly of N-type Ca^{2+} and BK channels underlies functional coupling in rat brain. *J. Cell Sci.* 120:985–995.

41. Marrion, N. V., and S. J. Tavalin. 1998. Selective activation of Ca^{2+}-activated K^+ channels by co-localized Ca^{2+} channels in hippocampal neurons. *Nature.* 395:900–905.

42. Berkefeld, H., and B. Fakler. 2008. Repolarizing responses of BKCa-Cav complexes are distinctly shaped by their Cav subunits. *J. Neurosci.* 28:8238–8245.

43. Marcantoni, A., P. Baldelli, J. M. Hernandez-Guijo, V. Comunanza, V. Carabelli, et al. 2007. L-type calcium channels in adrenal chromaffin cells: role in pace-making and secretion. *Cell Calcium.* 42:397–408.

44. Beeler, G. W., and H. Reuter. 1977. Reconstruction of the action potential of ventricular myocardial fibres. *J. Physiol.* 268:177–210.

45. Wang, Y.-W., J. P. Ding, X.-M. Xia, and C. J. Lingle. 2002. Consequences of the stoichiometry of *Slo1* α and auxiliary β subunits on functional properties of BK-type Ca^{2+}-activated K^+ channels. *J. Neurosci.* 22:1550–1561.

46. Horrigan, F., and R. Aldrich. 2002. Coupling between voltage-sensor activation, Ca^{2+} binding and channel opening in large conductance (BK) potassium channels. *J. Gen. Physiol.* 120:267–305.

47. Cox, D. H., J. Cui, and R. W. Aldrich. 1997. Allosteric gating of a large conductance Ca-activated K^+ channel. *J. Gen. Physiol.* 110:257–281.

48. Ding, J., and C. Lingle. 2002. Steady-state and closed-state inactivation properties of inactivating BK channels. *Biophys. J.* 82:2448–2465.

49. Zeng, X.-H., X.-M. Xia, and C. J. Lingle. 2003. Redox-sensitive extracellular gates formed by auxiliary β subunits of calcium-activated potassium channels. *Nat. Struct. Biol.* 10:448–454.

50. Lingle, C. J., X.-H. Zeng, J.-P. Ding, and X.-M. Xia. 2001. Inactivation of BK channels mediated by the N-terminus of the β3b auxiliary subunit involves a two-step mechanism: possible separation of binding and blockade. *J. Gen. Physiol.* 117:583–605.

51. Solaro, C. R., J. P. Ding, Z. W. Li, and C. J. Lingle. 1997. The cytosolic inactivation domains of BK_i channels in rat chromaffin cells do not behave like simple, open-channel blockers. *Biophys. J.* 73:819–830.

52. Benzinger, G. R., X. M. Xia, and C. J. Lingle. 2006. Direct observation of a preinactivated, open state in BK channels with β2 subunits. *J. Gen. Physiol.* 127:119–131.

53. Wallner, M., P. Meera, and L. Toro. 1999. Molecular basis of fast inactivation in voltage and Ca^{2+}-activated K^+ channels: a transmembrane β-subunit homolog. *Proc. Natl. Acad. Sci. USA.* 96:4137–4142.

54. Meinrenken, C. J., J. G. Borst, and B. Sakmann. 2003. Local routes revisited: the space and time dependence of the Ca^{2+} signal for phasic transmitter release at the rat calyx of Held. *J. Physiol.* 547:665–689.

55. Wu, Y. C., and R. Fettiplace. 1996. A development model for generating frequency maps in the reptilian and avian cochleas. *Biophys. J.* 70:2557–2570.

56. Shao, L. R., R. Halvorsrud, L. Borg-Graham, and J. F. Storm. 1999. The role of BK-type Ca^{2+}-dependent K^+ channels in spike broadening during repetitive firing in rat hippocampal pyramidal cells. *J. Physiol.* 521:135–146.

57. Zeng, X. H., X. M. Xia, and C. J. Lingle. 2005. Divalent cation sensitivity of BK channel activation supports the existence of three distinct binding sites. *J. Gen. Physiol.* 125:273–286.